Sellers, D. *SIAM J. Appl. Math.* **1967**, *15*, 13.
Shinnar, R.; Fortuna, G.; Shapira, D. *Ind. Eng. Chem. Process Des. Dev.* **1982**, *21*, 728.
Shinnar, R. *Ann. N.Y. Acad. Sci.* **1983**, *404*, 432.
Wei, J.; Prater, C. D. *Adv. Catal.* **1962**, *13*, 204.
Wei, J. *J. Catal.* **1982**, *76*, 433.
Weize, P. W.; Frillette, V. J. *J. Phys. Chem.* **1960**, *69*, 382.

Received for review October 25, 1982
Revised manuscript received May 29, 1984
Accepted November 19, 1984

Fluid Mechanics of Mixing in a Single-Screw Extruder

Ravindran Chella and Julio M. Ottino*

Department of Chemical Engineering, University of Massachusetts, Amherst, Massachusetts 01003

An analysis is presented of mixing in cavity flows and in the single-screw extruder, valid for realistic degrees of mixing (stretching). The limitations of conventional numerical tracking schemes and the general characteristics of flows with weak reorientation are discussed. The analysis gives insight into the physics of the process and suggests ways for improved operation by highlighting the role of operating conditions, the mode of feed introduction, and the role of mixing sections.

Introduction

The objective of this work is to present and analyze a detailed physical model of mixing in a single-screw extruder. For simplicity our results will be presented in terms of a Newtonian fluid, but the extension to other constitutive models should be clear. When possible, our results will be compared with experimental observations and other theoretical analyses. However, one of the main problems of mixing research is the almost total absence of systematic experimental work. (For a review of laminar mixing of polymeric fluids see Ottino and Chella, 1983; the existing experimental work relevant to extruders is reviewed by Arimond, 1984.) From a general viewpoint, there are two principal conceptual problems: (i) how to measure mixing, and (ii) how to implement the measure, i.e., to relate the mixing measure to the velocity field. It is desirable that the analysis be valid, without breakdown or unreasonable computational requirements, up to realistic degrees of mixing.

Usually the starting point for the mixing of immiscible fluids is a two-phase system consisting of thick striations or large blobs. Mechanical mixing causes the striation thicknesses to decrease by several orders of magnitude (10^4). A decrease in length scales of segregation from centimeters to microns is reasonable, and eventually breakup into droplets or ribbons will occur (Figure 1). The stretching and breakup are related in a complicated way to the velocity field.

According to Aref and Tryggvason (1984), the mixing of immiscible fluids may be conveniently divided into two classes: mixing with *passive* and *active* interfaces. For passive interfaces, the motion is *topological*; i.e. there is no breakup, and the interfaces act as markers of the flow. In particular, this is the case of mixing of two immiscible fluids having similar properties and negligible interfacial tension. For active interfaces, generally occurring at small scales where interfacial forces become important, the interfaces interact with the flow and modify it. A conceptual representation of this process is shown in Figure 1. It is convenient to describe mixing in terms of deformation and stretching of passive interfaces and then to add at a small scale the effect of active interfaces (Khakhar et al., 1984).

Given these definitions, the scope of this work (a) and its possible generalizations (b) are given respectively as follows: (1) (a) similar Newtonian fluids; (b) non-Newtonian fluids: trivial provided that the velocity field can be obtained; (2) (a) passive interfaces; (b) active interfaces: deformation and breakup can be added at a small scale (see Khakhar et al., 1984); (3) (a) immiscible fluids; (b) diffusing and reacting fluids: can be treated in terms of the lamellar model (see Chella and Ottino, 1982, for reactions in an extruder; different reaction schemes are treated by Chella and Ottino, 1984).

There are several goals to the present work. In a narrow sense the objective is to use the single-screw extruder, a prototype case of mixing in a reasonably complicated flow field, as a test ground for the application of the lamellar mixing model (Ottino et al., 1981). However, the byproducts of the application are equally important. We provide new insights into the physics and guidance for improved operation. We will be able to compare our approach with other methods: the use of *Weighted Average Total Strain* (WATS) to model mixing in extruders, the *Marker-and-Cell technique* (MAC) to describe mixing in cavity flows, and general numerical methods based on tracking interfaces by means of small displacements.

The Marker-and-Cell technique provides a good means of dispelling a commonly held belief *that once the velocity field is obtained, the mixing problem is essentially solved.* This is far from being true, and actually fairly simple, deterministic, flows can lead to extremely intricate, *chaotic*, mixing patterns (Aref, 1984; Khakhar et al., 1984). Although we do not consider chaotic mixing here, calculating large degrees of mixing in the extruder flow can easily exceed computational limits.

Laminar Mixing

One of the earliest theoretical treatments of laminar mixing was by Spencer and Wiley (1951). They found that the deformation of an interface subject to large unidirectional shear is proportional to the imposed strain, the proportionality constant being a function of the initial orientation. This result has been empirically extrapolated to the analyses of mixing in the extruder (Mohr et al., 1957; McKelvey, 1962; Pinto and Tadmor, 1970; Erwin, 1978).

0196-4313/85/1024-0170$01.50/0

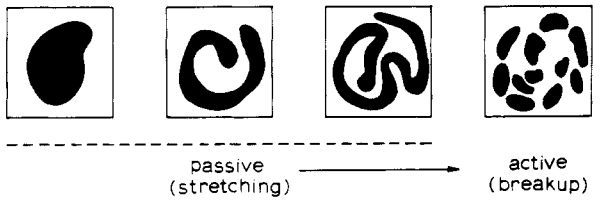

Figure 1. Schematic of general mixing problem.

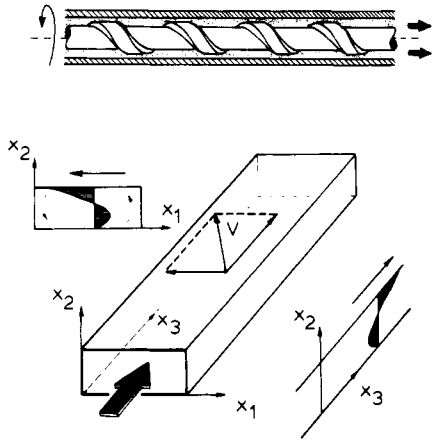

Figure 2. Schematic diagram of single-screw extruder and rectangular channel model.

In particular, the Weighted Average Total Strain (WATS), a measure which accounts for the distribution of strain histories among the fluid elements, relies on this assumption (Pinto and Tadmor, 1970; Tadmor and Klein, 1970). This approach is computationally simple and provides semiquantitative information on the influence of model parameters on mixing; however, it suffers from several disadvantages: (i) it is difficult quantitatively to relate the strain measure to any experimentally accessible measure of mixing (see Bigg and Middleman, 1974a); (ii) the analogy to large unidirectional shear appears to be an oversimplification of the complex flow field in the extruder and can mask details of the mixing mechanism; (iii) the lack of explicit consideration of intermaterial orientation precludes a systematic analysis of the mode of feed introduction or different types of mixing sections; and (iv) only mean values are obtained. Information about the distribution of mixedness may be important when simultaneous diffusion and reaction occur.

Recently, Erwin and Mokhtarian (1983) analyzed mixing in extruders by means of the Marker-and-Cell technique and compared their results with the experimental results of Gailus and Erwin (1981). They are able to simulate the effect of mixing sections and to compute stretch ratios up to 10^2.

Flow Characteristics of the Single-Screw Extruder

The single-screw extruder consists of a screw with a shallow helical channel cut on its side rotating inside a cylindrical barrel (Figure 2). Under normal operating conditions in polymer processing applications—large aspect ratios and low Reynolds numbers—the system can be modeled, for purposes of fluid mechanical analysis, as a stationary channel with an upper plate moving diagonally across the top at an angle θ (helix angle) to the axis x_3 (McKelvey, 1962). See Figure 2. Fluid is conveyed forward along the channel by the axial component of the drag flow induced by the motion of the plate, while a pressure flow builds up in the reverse direction due to the resistance offered by the die at the outlet. While the extruder throughput and pressure drop are largely influenced by the axial flow, it is the transverse flow, generated by the drag flow component in that direction, that is primarily responsible for the mixing action of the extruder. A fluid element undergoes deformation in its helical path through the channel, the helix angle at any point being determined by the local velocity field.

Tadmor and Klein (1970) have reviewed several models for the extruder flow field. The "simplified flow theory" (SFT) of Carley et al. (1953) is one of the most popular by virtue of its simplicity and good agreement with experimentally determined *throughput* and *pressure drop* measurements. End effects at the flights are neglected, to obtain for the fully developed velocity profile

$$v_1 = x_2(2 - 3x_2) \tag{1a}$$

$$v_2 = 0 \tag{1b}$$

$$v_3 = x_2[1 + 3\phi(x_2 - 1)] \tag{1c}$$

The suitability of this flow for mixing studies has not been clearly established. Equations 1, independent of x_1, do not predict a "smooth" helical motion of fluid particles in the extruder channel; instead, a fluid particle is constrained to travel in its own "horizontal" plane (x_2 = constant) until it encounters the flights. Subsequently, it continues its motion in a complementary horizontal plane with the x_1 component of its velocity reversed. However, most analyses of mixing using WATS (Pinto and Tadmor, 1970; Erwin, 1978) are based on this velocity field.

Clearly this velocity field is invalid in the neighborhood of the flights and is useful only for large aspect ratios. Assumptions are necessary regarding the changes in orientation and stretch of the material elements at the flights. The sensitivity of the results to these assumptions is an important factor in determining the usefulness of this particular flow description. The SFT will be used in the initial mixing analysis, with refinements made if and when they prove necessary.

Basic Equations and General Results

The area stretch, η, orientation, $\hat{n}$, and specific rate of stretching, α, of a differential material surface at time t, subject to an arbitrary topological motion, can be related to the initial orientation $\hat{N}$ and the fluid motion through the kinematic relations (see Ottino et al., 1981)

$$\eta = (\mathbf{C}^{-1}:\hat{N}\hat{N})^{1/2} \tag{2a}$$

$$\hat{n} = (\mathbf{F}^{-1})^T\cdot\hat{N}/\eta \tag{2b}$$

$$\alpha(\boldsymbol{X},t) = \dot{\eta}/\eta = -\mathbf{D}:\hat{n}\hat{n} \tag{2c}$$

The specific rate of stretching, α, is bounded by the quantity $(\mathbf{D}:\mathbf{D})^{1/2}$. This gives rise to the *mixing efficiency*

$$e(\boldsymbol{X},\hat{N},t) = \frac{\dot{\eta}/\eta}{(\mathbf{D}:\mathbf{D})^{1/2}} = \frac{\text{actual rate of stretching}}{\text{upper bound}} \tag{3}$$

Several characteristic features of the behavior of α and e can be identified (Figure 3). In many bounded flows α decays as t^{-1} for long times (Figure 3a). Such behavior is characteristic of all *steady curvilinear flows* (Chella, 1984). In flows with moderate reorientation, α consists of a succession of t^{-1} decaying flows; the time-average of α decays to zero (Figure 3b). In flows with strong reorientation the efficiency oscillates without decaying; the time-average of α is constant. This behavior is characteristic of flows with strong reorientation and chaotic flows (Figure 3c; Khakhar et al., 1984).

When the motion is topological, the resulting structure is lamellar. Locally, the intermaterial area density, a_v, or the striation thickness, $s(t)$, provide quantitative measures

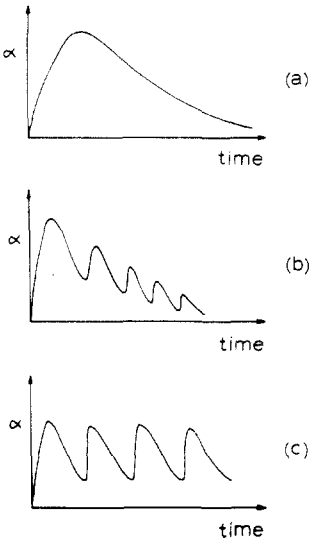

Figure 3. Characteristic behavior of flow mixing efficiencies: (a) no reorientation; (b) weak reorientation; (c) strong reorientation.

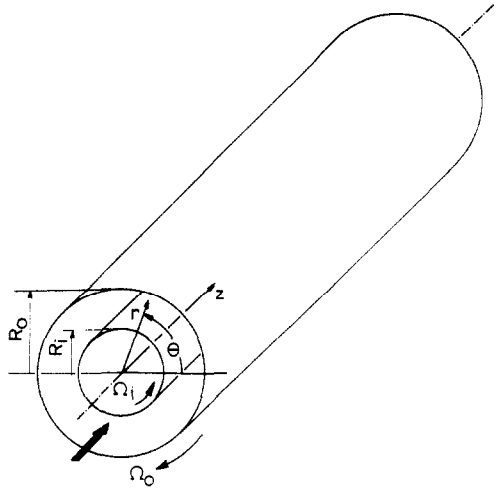

Figure 4. Schematic diagram of helical annular mixer.

of the state of mixedness. For isochoric motions, local values of a_v can be simply related to local values of the area stretch, η, by (Ottino, 1982)

$$a_v = a_v^0 \eta \tag{4}$$

Before attempting to model the mixing mechanisms in the complex flow field of the extruder, it is helpful to consider its building blocks. The *helical annular mixer* typifies the ratio of transverse to axial flow, whereas the *cavity flow* mimics the transverse flow in the extruder.

Helical Annular Mixer

The helical annular mixer (Figure 4) has been studied both experimentally and theoretically (using ad hoc geometric arguments) by Schrenk et al. (1963). A more general analysis is presented in Ottino and Chella (1983); some results relevant to the analysis of mixing in the extruder are given here (for the case of inner cylinder rotating and the outer cylinder stationary, analogous to the situation in the extruder).

Using the relations of the previous section with the velocity field of Schrenk et al. (1963) for this mixer, we have

$$\eta = [1 + zA(EF_1N_\theta + F_2N_z)(zAEF_1N_\theta + zAF_2N_r - 2N_r)]^{1/2} \approx zA(EF_1N_\theta + F_2N_z); \quad (\text{for } zA \gg 1) \tag{5}$$

where F_1, F_2 are functions of r and $K(= R_i/R_0)$.

When the feed is introduced with radial interfaces ($N_\theta = 1$, $N_r = N_z = 0$), eq 5 reduces to

$$\eta = [1 + (zAEF_1)^2]^{1/2} \approx zAEF_1; \quad (\text{for } zAE \gg 1) \tag{6}$$

This is the same relation as that obtained by Schrenk et al. (1963) if η ($= a_v/a_v^0$) is interpreted as $(s/s_0)^{-1}$. Schrenk et al. (1963) obtained excellent experimental confirmation of their theoretical predictions for the mixing of pigmented polystyrenes.

The striation thickness distribution is nearly symmetric between the cylinders. As $K \to 1$ it can be shown that

$$\left(\frac{s}{s_0}\right)_{max} \approx \frac{3}{2zAE}(1 - K) \tag{7}$$

i.e., the maximum striation thickness decreases linearly with axial distance.

The RTD of the helical annular mixer is relatively narrow and resembles that of the single-screw extruder. The mixing-cup average of η in the helical annular mixer can be obtained as

$$\langle\langle\eta\rangle\rangle \approx \left\langle\left\langle\frac{s}{s_0}\right\rangle\right\rangle^{-1} \approx 4zA\left\{N_\theta E\left[\frac{K^2}{(1-K^2)^2}\ln\left(\frac{1}{K}\right)\right] + \frac{N_z}{3(1+K)}\left[2 + \frac{K_2(K_1+2K)}{2}\right]\right\}; \quad (\text{for } zA \gg 1) \tag{8}$$

$$\approx zA\left\{\frac{N_\theta E}{(1-K)} + N_z\right\}; \quad (\text{as } K \to 1)$$

In similar fashion, the mixing achieved in a pure Couette flow (the transverse flow in the helical annular mixer) can be shown to be

$$\eta_{\text{Couette}} = \left\{1 + \frac{4\pi nK^2}{(1-K^2)}\frac{N_\theta}{r^2}\left[\frac{4\pi nK^2}{(1-K^2)}\frac{N_\theta}{r^2} - 2N_r\right]\right\}^{1/2} \approx \frac{4\pi nK^2}{(1-K^2)}\frac{N_\theta}{r^2}; \quad (\text{for } n \gg 1) \tag{9}$$

where n is the number of revolutions of the rotating inner cylinder. The cross-sectional-averaged value of the striation thickness is given by

$$\overline{\left(\frac{s}{s_0}\right)^{-1}}_{\text{Couette}} = \bar{\eta}_{\text{Couette}} \approx \frac{8\pi nK^2}{(1-K^2)}\ln[1/K]N_\theta \tag{10}$$

Thus on comparing eq 8 and 10 with zAE ($= z\Omega\bar{t}$) interpreted as equivalent to $2\pi n$, the first term on the right-hand side of eq 8 corresponds to the mixing effect of the *transverse Couette flow*. The second term corresponds to the mixing effect of the *axial Poiseuille flow*. The important result is that for narrow annuli ($K \to 1$), or for $E \gg 1$, the transverse flow term dominates the mixing in the helical annular mixer for most feed conditions of interest ($N_\theta \neq 0$). Also it can be shown that the helical annular mixer is a flow without reorientation (Figure 3a). The overall mixing efficiency for striation thickness reduction of 10^2–10^3 is of $O(1\%)$.

The helical annular mixer provides an idea of the relative contributions to mixing of the transverse and axial flows which might be expected in the extruder. However, the transverse flow in the extruder is inherently different from a Couette flow; hence the transverse flow in the extruder, the rectangular cavity flow, is examined in greater detail.

Rectangular Cavity Flow

Figure 5 is a diagram of a sequence of steps in the stretching of an interface that has been subjected to two-dimensional rectangular cavity flow. The increase in

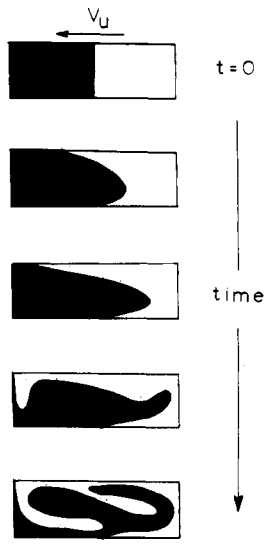

Figure 5. Schematic diagram of sequence of steps in the stretching of an interface between two adjacent vertical fluid layers in two-dimensional rectangular cavity flow.

length of the interface, $L(t)$, is accompanied by a decrease in the striation thickness, defined as the average perpendicular distance between neighboring interfaces, so that for long times $L(t)\cdot s(t) \approx$ constant. Biggs and Middleman (1974b) used a simplified Marker-and-Cell (MAC) technique (Harlow and Amsden, 1970) to track the position of the interface. However, they only considered the case where the interface was horizontal, and they assumed small stretch ratios.

In a typical numerical simulation, the deformation and stretching of continuous lines (or surfaces) is modeled using a finite number of particles. For a relative stretch of one or two orders of magnitude as the line deforms the individual particles comprising the line separate, making the line less clearly defined. For every initial concentration of particles (number of particles per unit length) there will be a time beyond which it becomes nearly impossible to reconstruct the line. (This problem is magnified dramatically if the flow is chaotic.) An identical problem arises in experimental work when a line is simulated in terms of tracer particles. On the other hand, the line cannot be too concentrated as it would not behave as a passive interface. If the line is simulated in terms of a soluble tracer, the problem is diffusion. In general, it appears to be extremely difficult to follow stretching by conventional tracking techniques and/or experiments for relative stretch ratios of order 10^2 or higher. Numerical errors might make it impossible to achieve the reversibility expected from *regular* motions (Khakhar et al., 1984).

The change in length of the interface may be calculated using the relation for the stretching of a finite material line

$$L(t) = \int_{L(0)} (\mathbf{C}:\hat{M}\hat{M})^{1/2}|d\mathbf{X}| \qquad (11)$$

The set of initial orientations of the differential line elements comprising the interface need to be specified. For a vertical interface (perpendicular to the moving plate) $\hat{M}$ = (0,1), and for a horizontal interface (parallel to the moving plate) $\hat{M}$ = (1,0), for all the line elements. The evaluation of the integral in eq 11 is relatively simple as it is over the *initial configuration*. The approach used here can be carried out to *arbitrarily large stretch ratios*.

In order to apply eq 11, a mathematical description of the cavity flow field is needed. The error involved in the use of a steady-state velocity profile for an essentially transient problem is relatively small in this case, as

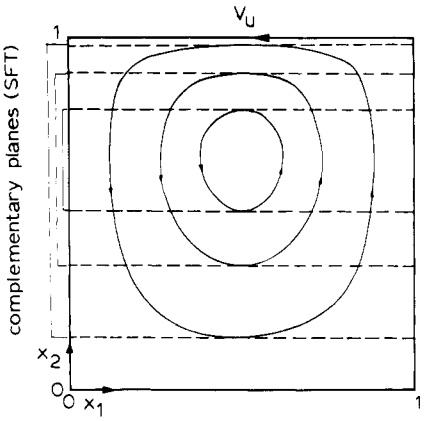

Figure 6. Comparison of streamlines for rectangular cavity flow obtained using the SFT (---) and eq 12 for W/H = 15.

steady-state operating conditions are rapidly attained under normal operating conditions (Bigg and Middleman, 1974b; Erwin and Moktharian, 1981). The simplest such description for this flow is that given by eq 1.

However, in using eq 1 in conjunction with eq 11 to determine $L(t)$, assumptions are necessary regarding the changes in orientation and deformation undergone by a material element in moving to its complementary location. However, computations indicate that *the mixing achieved is extremely sensitive to the assumed change in orientation at the flights*. It is therefore desirable to develop a mathematical description of the flow field that does not entail such arbitrary assumptions. While a numerical solution to the Navier–Stokes equations for this flow field (eq A.1, 2) is possible, it does not seem feasible to compute stretch ratios of order 10^3 or higher based on current tracking techniques. Additionally, a semianalytical treatment allows for easier visualization of the effect of different parameters. Hence, in the Appendix, the Kantorovich–Galerkin method (Kantorovich and Krylov, 1964) is used to obtain an approximate analytical steady-state, creeping flow solution to the cavity flow equations. From eq A.8, A.15, and A.22

$$v_1 = \frac{21}{\epsilon}x_1^2(1-x_1)^2\{A_2[(\delta_1^2+\delta_2^2)/\delta_1]\sinh(\delta_1x_2)\sin(\delta_2x_2) + B_1[\delta_2\sinh(\delta_1x_2)\cos(\delta_2x_2) + \delta_1\cosh(\delta_1x_2)\sin(\delta_2x_2)]\} \qquad (12a)$$

$$v_2 = 42x_1(1-x_1)(1-2x_1)[A_2\cosh(\delta_1x_2)\sin(\delta_2x_2) + B_1\sinh(\delta_1x_2)\sin(\delta_2x_2) + B_2\sinh(\delta_1x_2)\cos(\delta_2x_2)] \qquad (12b)$$

where A_2, B_1, and B_2 are functions only of the cavity aspect ratio, defined in eq A.22.

Even though these equations satisfy the boundary condition on the velocity at the moving plate only in the mean, the streamlines calculated using them are in good agreement, for large aspect ratios, with those obtained by more accurate numerical methods (Pan and Acrivos, 1967); also, the maximum and minimum x_2 coordinates of the streamlines coincide almost exactly with the location of the corresponding complementary plants of the SFT (Figure 6).

The relative stretch experienced by an initially vertical interface, calculated using eq 11 and 12, is shown in Figure 7 for two different aspects ratios. The aspect ratio has only a small influence on the relative stretch of the interface; the period of oscillation of the curves about a monotonically increasing mean value is approximately equal to V_U/H, a characteristic recirculation time. The periodic oscillation can be seen more clearly in Figure 8, where the

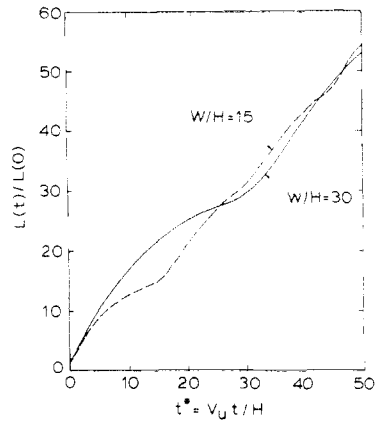

Figure 7. Relative stretch of interface in rectangular cavity flow as a function of the channel aspect ratio, calculated with the velocity field of eq 12, for an initially vertical interface (perpendicular to the moving plate) dividing cavity into equal volumes.

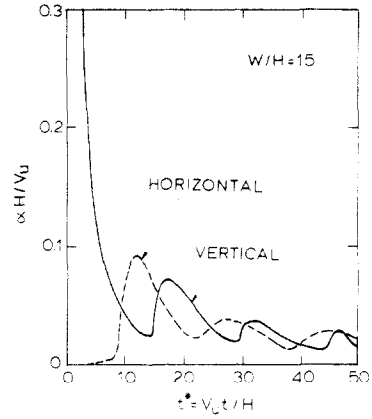

Figure 8. Nondimensionalized specific rate of stretching of interface in rectangular cavity flow (W/H = 15, initially vertical interface).

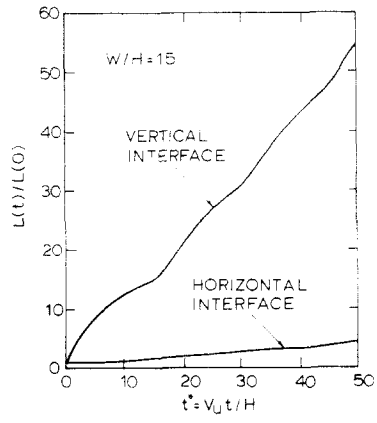

Figure 9. Influence of initial orientation on relative stretch of interface in rectangular cavity flow (W/H = 15).

specific rate of stretching of the interface $\alpha(= \mathrm{d} \ln L(t)/\mathrm{d}t)$ plotted vs. time shows the same characteristic oscillation. Thus the cavity flow has weak reorientation (Figure 3b).

The influence of the initial orientation of the interface on the normalized interface length is shown in Figure 9. The apparent sensitivity of the mixing level to the initial orientation is an artifact of choice of coordinates in Figure 9. When the actual amount of interfacial area in each case is calculated, the dependence on the initial orientation is found to be very small. The reason for this can be seen in Figure 8, where the initial large differences between an initially vertical interface (almost perpendicular to the flow streamlines) and an initially horizontal interface (almost parallel to the flow streamlines), narrows considerably as

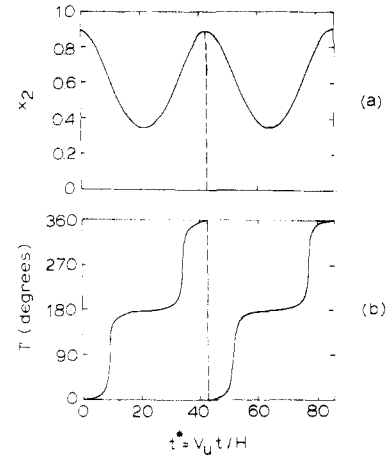

Figure 10. Change in elevation (a) and orientation (b) of a differential material element in traveling along a streamline in rectangular cavity flow, calculated with the velocity field of eq 12 (Γ is the angle between the normal to the material plane and the x_1 axis).

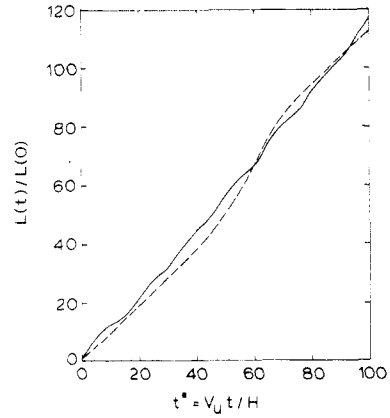

Figure 11. Comparison of interface stretching in rectangular cavity flow predicted by the SFT (----) with that predicted using the flow field of eq 12 (—), (W/H = 15, initially vertical interface).

more and more of the initially vertical interface becomes aligned horizontally. Also, mixing is found to be relatively insensitive even to large displacements in the initial location of the interface.

The relative stretch of the interface can be approximated by the relation

$$\frac{L(t)}{L(0)} \doteq \left[\frac{s(t)}{s(0)}\right]^{-1} \approx 1 + 0.625\frac{V_U t}{L(0)} \qquad (13)$$

While the use of the velocity field given by eq 12 in the analysis of mixing in the extruder involves no additional conceptual difficulty, the computational effort is considerably increased compared with the SFT. Hence it is useful to determine whether information obtained with this flow field regarding the change in orientation of the fluid elements near the flights can be incorporated into mixing calculations using the SFT with satisfactory results.

Figure 10 shows a typical plot of the change in orientation of a differential line element with time. Also indicated, in the upper portion of the figure, are the corresponding x_2 coordinates of the element (Figure 10a), the dashed lines indicating the locations of the maximums and the minimums. The pattern shown here is found to quickly establish itself regardless of the initial location or orientation of the material element. Thus the material elements are rotated through nearly 180° while reversing their x_1 flow direction near the boundaries. The usefulness of the SFT in making predictions of mixing with the material elements assumed to rotate through 180° at the

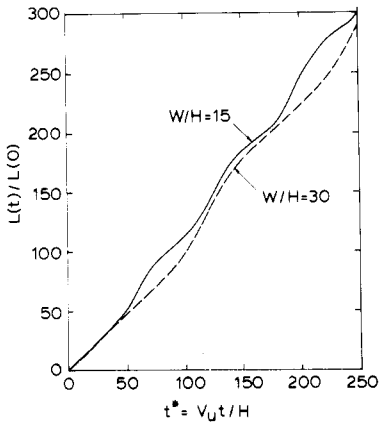

Figure 12. Influence of cavity aspect ratio on stretching of an initially vertical interface in rectangular cavity flow as predicted using the SFT.

boundaries is now examined.

The deformation of an initially vertical interface calculated using the SFT, with the fluid elements rotated through 180° at the flights, is compared to that calculated using eq 12, in Figure 11. Numerically the two curves are in good agreement; however, the period of the oscillation obtained using the SFT is more than three times that obtained using eq 12 and is approximately in agreement with the value of the redistribution time (defined by Shearer (1973) as the time required to displace fluid completely from one side of the cavity to the other) calculated using the SFT

$$t^*_{redis} = \frac{27}{8}\frac{W}{H} \tag{14}$$

The agreement between the mixing predictions for an initially vertical interface using these two different flow fields, even for the relatively large stretch ratios shown in Figure 11, seems rather surprising as the SFT predicts no deformation of a horizontal interface, and a large portion of the interface is nearly horizontal at these large stretch ratios. However, for finite times the interface is never perfectly horizontal, and the SFT predicts a small but finite stretch in agreement with the predictions of eq 12.

The weak dependence of the mixing achieved on the channel aspect ratio predicted using eq 12 is confirmed using the SFT (Figure 12). The SFT with the 180° rotation of the material elements at the flights is thus seen to duplicate the principal features of mixing in the rectangular cavity flow as predicted using eq 12, and its use in the analysis of mixing in the three-dimensional extruder flow is favored over eq 12 because of its relative simplicity.

Comparison of the theoretical predictions with experimental data is difficult because of a scarcity of experimental data. The available experimental data are incomplete (e.g., Bigg and Middleman, 1974b) both because of the uncertainity about whether two-dimensional flow was achieved in the experimental setup and because not many data were taken under conditions of interest here (large aspect ratios). However, a comprehensive experimental program is underway (Chien, 1984).

The conclusions obtained from the cavity flow should be applied with care to extruders. It should be noted that the distribution of velocities across the extruder cross-section prevents an exact coordinate transformation between successive times in the rectangular cavity and axial distance along the extruder. Also, from a topological point of view, if we consider the mixing of two fluids, say A and B, initially layered horizontally in the cavity flow, the two contact lines at the side wall are present throughout the entire motion. However, an extruder filled initially with A and subsequently fed with A and B as adjacent horizontal layers would have A wetting and boundaries completely, with no contact lines. An analogous situation is obtained for a vertical interface.

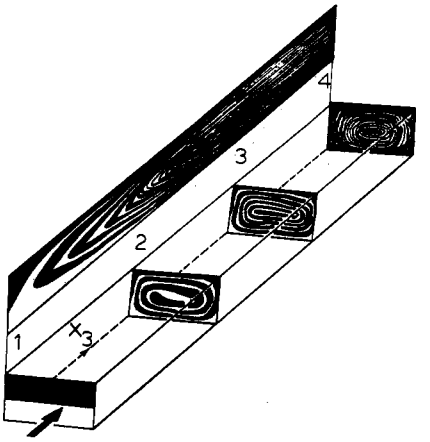

Figure 13. Schematic diagram of lamellar structure generated by the extruder flow field in the mixing of two fluids introduced as adjacent horizontal layers.

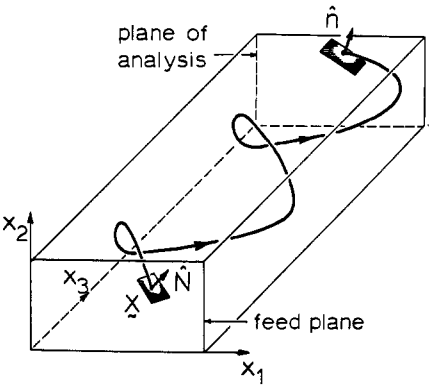

Figure 14. Pathline of material elements in extruder channel.

From the above arguments it is apparent that no rigorous extension of the approach used to analyze mixing for the two-dimensional cavity flow is possible to the three-dimensional extruder flow; however, the possibility of approximate relations will be explored.

Analysis of Mixing in Single Screw Extruder

The approach used to analyze mixing in the extruder is similar in principal to that used for the helical annular mixer; modifications are necessary, however, as a completely analytical approach is not possible using the velocity field given by eq 12 and is precluded for the SFT by the discontinuities in the fluid element pathlines at the flights.

Figure 13 is a diagram of the mixing of two fluids in the extruder channel. Cross-sectional cuts and an axial cut display the layered structure generated by the mixing action. As for the helical annular mixer, a_v and s are used as local measures of the state of mixedness. The distributions of the mixing parameters a_v and α at any channel cross section correspond to the nonhomogeneity of the flow field and to distributions in the orientations and thicknesses of the striations in the feed plane. For many applications it should be sufficient to characterize these distributions by their first few moments.

Axial profiles of the means and moments of the cross-sectional mixing parameter distributions can be determined as follows (see Figure 14): (i) A number of differential material planes are identified in the feed plane,

the location and orientation of each corresponding to the position of the interfacial area in the feed. The number of planes chosen should be large enough that the influence of this variable on the calculated distributions is negligible; the actual number, of course, depends on the mixing achieved; in practice, 200–300 elements were found to be sufficient for a three order of magnitude decrease in the striation thickness. Note that the RTD was found to be much less sensitive than the mixing parameter distributions to the number of material elements chosen. (ii) Equations 2 are used in conjunction with a mathematical description of the flow field to calculate the stretch histories of each of these material planes. (iii) The mean and moments of the mixing parameter distributions are determined at several axial locations. This method is very general and can be applied to other mixers.

The macroscopic mixing efficiency for continuous flow systems is defined by the relation (Ottino et al., 1981)

$$\langle\langle \ln a_v \rangle\rangle_0^z = (\mathrm{eff}(z))_0^z \frac{\overline{(\mathbf{D}:\mathbf{D})}^{1/2}}{\bar{v}_z} z \qquad (15)$$

Before resorting to more detailed calculations, it is instructive to examine the upper mixing bound, obtained by setting eff(z) = 1 on the right-hand side of eq 15. Typically, the upper mixing bound predicts values significantly higher than are achieved in most practical mixing flows (Ottino and Macosko, 1980; Ottino, 1983), but provides an indication of the influence of model parameters on mixing.

Computation of the upper mixing bound is particularly simple for the SFT.

$$\langle\langle \ln a_v(z) \rangle\rangle_0^f \leq \frac{[4 - 3(1 - \phi^2)\cos^2\theta]}{(1 - \phi)\sin(2\theta)} \left(\frac{L}{H}\right) \qquad (16)$$

The proportionality constant required for equality is a function of the feed orientations $\{\hat{N}\}$, and of ϕ, θ, and L/H (through their influence on the mean residence time). Thus from eq 16, the relevant parameters that influence mixing are $\{\hat{N}\}$, ϕ, θ, and L/H. The influence of W/H arises only indirectly through the change in the vertical coordinate of the fluid elements at the flights.

On the basis that when the upper bound increases, there is a possibility of improved mixing, then from eq 16, mixing may be improved by: (i) increasing ϕ at constant L/H and θ; (ii) increasing L/H at constant θ and ϕ; (iii) increasing θ for $\theta > \theta_{min}$, decreasing θ for $\theta < \theta_{min}$, at constant L/H and ϕ, where

$$\theta_{min} = \tan^{-1} \frac{(1 + 3\phi^2)^{1/4}}{2^{1/2}} \qquad (17)$$

and

$$\frac{\pi}{6} \leq \theta_{min} \leq \frac{\pi}{4}$$

and (iv) decreasing H at constant L/H and θ.

These conclusions are in agreement with qualitative experimental observations (Maddock, 1959; Sheridan, 1975) and will be tested using a more complete analysis in the next section.

Results and Discussion

Inspection of the model equations indicates the parametric dependence of $\langle\langle \eta \rangle\rangle$ to be

$$\langle\langle \eta \rangle\rangle = f(L/H, \theta, \phi, \{\hat{N}\}) \qquad (18)$$

The sensitivity of the mixing to each of these parameters provides guidance with regard to design and operation.

As noted in the previous section, the SFT, with material elements rotated through 180° at the flights, duplicates

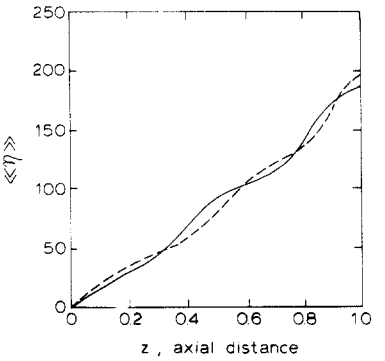

Figure 15. Comparison of area stretch along the extruder, calculated using the SFT (—) and eq 12, A.6 (- - -); (L/H = 15, W/H = 15, ϕ = 0.3, vertical feed interface).

the principal features of the mixing predictions of the more complete flow field given by eq 12 for the transverse flow in the extruder. Also the axial profiles of $\langle\langle \eta \rangle\rangle$ along the extruder calculated using eq 12 together with eq A.6 for the axial velocity profile are in good agreement with values obtained using this version of the SFT (see e.g., Figure 15). Thus subsequent computations are carried out using the SFT, its use being favored because of its relative simplicity. As expected, the single-screw extruder behaves as a mixing flow with weak reorientation (Figure 3b).

The values of $\langle\langle \eta \rangle\rangle$ calculated using the coordinate transformation

$$t = z\bar{t} \qquad (19)$$

between successive times in the rectangular cavity flow and axial distance along the extruder are in excellent agreement with the corresponding values obtained by the more exact procedure detailed earlier (points (i) through (iii) above). This confirms the expectation, by analogy with the helical annular mixer, of a relatively narrow distribution of mixing parameters (weighted for the flow) across the extruder cross section and the importance of transverse flow in determining the mixing characteristics of the extruder. As the RTD of the extruder (in normalized coordinates) for Newtonian fluids is virtually independent of the extruder's dimensions and operating conditions (Pinto and Tadmor, 1970; Bigg and Middleman, 1974a), the transformation given by eq 19 should be approximately applicable over a wide range of conditions. In this formulation, the dependence of the mixing achieved on these parameters arises through the functional dependence of $\bar{t}$.

$$\bar{t} = \frac{4L}{V_b \sin(2\theta)(1 - \phi)} \qquad (20)$$

Then, from eq 20 and the results obtained for the rectangular cavity flow, mixing is predicted to be relatively insensitive to the channel aspect ratio, W/H, and the channel helix angle, θ (except for small values of θ), and to be inversely proportional to $(1 - \phi)$ in agreement with the results obtained by examination of the upper mixing bound in eq 16.

The influence of some of the parameters in eq 18 on $\langle\langle \eta \rangle\rangle$ are shown in Figures 16–18. The dependence of $\langle\langle \eta \rangle\rangle$ on axial distance, z, along the extruder is nearly linear except for a small superimposed periodic oscillation about a mean value. This oscillation reflects the partial reorientation of the intermaterial surface at the flights. Mixing is relatively insensitive to ϕ for $\phi \leq 0.3$; beyong a value of about 0.7, mixing increases sharply with ϕ. The dashed lines in Figure 17 correspond to the predictions of the WATS approach. As WATS cannot be directly related to any physical measure of mixing, the dashed lines in

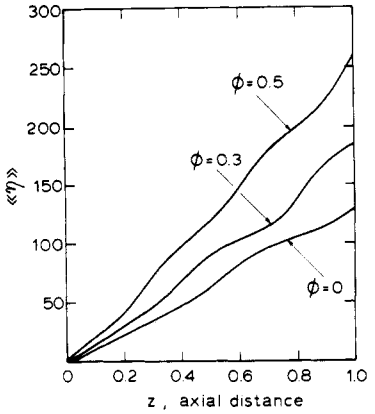

Figure 16. Influence of negative pressure to drag flow ratio (ϕ) on mixing in a single screw extruder (L/H = 50, W/H = 15, θ = 15, vertical feed interface).

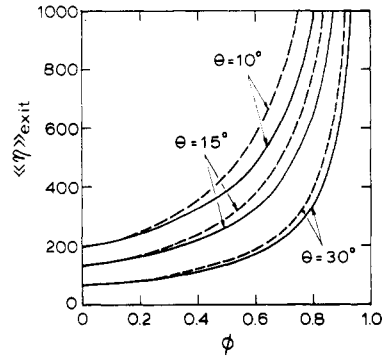

Figure 17. Influence of negative pressure to drag flow ratio (ϕ) and channel helix angle (θ) on mixing in a single screw extruder (L/H = 50, W/H = 15, vertical feed interface). The dashed lines correspond to the prediction of WATS (obtained by calibration with the ϕ = 0 value).

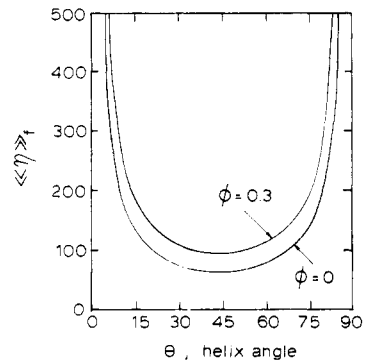

Figure 18. Influence of channel helix angle (θ) on mixing in a single screw extruder (L/H = 50, W/H = 15, vertical feed interface).

Figure 17 were obtained by calibration with the value of $\langle\langle\eta\rangle\rangle$ corresponding to ϕ = 0. The two models are in agreement for small values of ϕ, but show increasing deviation as ϕ increases. Note that the physical significance of the mixed-cup average value of the stretch is not very clear for values of $\phi > {}^1/_3$, when the axial velocity has a component in the negative axial direction.

For the range of θ values shown in Figure 17, which correspond to the range of channel helix angles commonly encountered, the influence of θ is largely to displace the curves, improved mixing being obtained with decreasing θ. However, in Figure 18, which shows the complete range of possible values of θ, a minimum in mixing is attained at a value of θ close to that predicted by eq 17.

The influence of the initial feed conditions is similar to that for the rectangular cavity flow. Mixing is relatively insensitive to the initial feed conditions.

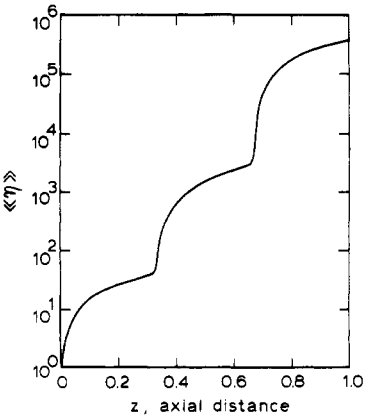

Figure 19. Effect of mixing sections located at $z = {}^1/_3$ and $z = {}^2/_3$ on mixing in a single screw extruder (L/H = 50, W/H = 15, θ = 15°, ϕ = 0.3, vertical feed interface).

The lack of effective orientation of the material elements at the flights causes the bulk of the interfacial area to be oriented parallel to the channel bottom in a relatively short downstream distance, regardless of the initial orientation. Consequently the mixing achieved in single screw extruders is generally poor (the extruder is a flow with weak reorientation, Figure 3b). This has led to the design of "mixing sections" to obtain improved mixing. Mixing sections are devices that disrupt the flow and improve the mixing efficiency of the flow by redistribution and reorientation of the intermaterial area at the expense of only a small increase in power. Here we consider mixing sections where randomization of interfacial planes occur. Other types of mixing sections can be modeled as planes where the material elements are assigned a particular orientation. The effect of pairs of mixing sections located equal axial distances apart is shown in Figure 19. Randomizing mixing sections are seen to greatly enhance mixing. The flow becomes a mixing flow with strong reorientation (Figure 3c). The effect of single pins acting as mixing sections is analyzed by Erwin and Mokhtarian (1983).

The axial variation of $\langle\langle\eta\rangle\rangle$ for the extruder exhibits similar behavior to that for the rectangular cavity flow. The overall mixing efficiency for this flow is also $O(1\%)$ for stretch ratios of order 10^2–10^3, but for a given mixing level the efficiencies are higher for the extruder than for the helical annular mixer.

Conclusions

The mixing characteristics of the single-screw extruder and the related simpler system, the helical annular mixer, are dominated by the transverse shear flow components. A significant difference between these mixers is that, except perhaps for a small initial region, the mixing efficiency of the helical annular mixer exhibits a monotonic z^{-1} decay, whereas in the extruder there is a periodic partial restoration of the mixing efficiency caused by the recirculation at the flights. The reorientation at the flights accounts for the higher efficiencies in the extruder.

The results of the previous sections on the dependence of mixing on the extruder dimensions and operating conditions are in general qualitative agreement with those of other theoretical analysis of mixing in extruders (Mohr et al., 1957; McKelvey, 1962; Pinto and Tadmor, 1970), but the approach used here allows for a quantitication of the mixing achieved in terms of experimentally accessible quantities, $\langle\langle s/s_0\rangle\rangle$ or $\overline{s/s_0}$. An approximate design relation for $\langle\langle s/s_0\rangle\rangle$ is

$$\langle\langle s/s_0\rangle\rangle^{-1} \approx 1 + 0.625\frac{L}{s_0}\frac{1}{\sin(2\theta)}\frac{z}{(1-\phi)} \qquad (21)$$

The values obtained for $\langle\langle s/s_0 \rangle\rangle$ are of the order of magnitude observed experimentally (cf. Han and Kim, 1975; Mohr et al., 1957; and particularly Gailus and Erwin, 1981); the available experimental work is, however, of a rather limited nature, and there is a need for more comprehensive experimental verification of the theoretical predictions.

The approach used here allows for a systematic treatment of the initial feed conditions, as well as internal flow redistribution devices such as mixing sections. Small degrees of taper in the extruder channel can be studied by using the lubrication approximation. Also the model can be easily extended to include simultaneous diffusion and reaction (see Chella and Ottino, 1982).

The restoration of efficiency at the flights in the single-screw extruder is very weak, and the mixing efficiency decays nearly inversely with axial distance along the extruder, behavior characteristic of shear flows. This would explain the qualitative agreement of the results obtained here with other theories based on mixing being proportional to the imposed shear. However, the theory here is applicable in general, even to mixers with substantial extensional flow characteristics (e.g., twin-screw extruders and static mixers), for which the other theories would be expected to fail.

The complications due to viscosity ratio, elasticity, and interfacial tension seem to increase in this order. Assuming the approximate validity of the coordinate transformation of eq 19, the results of Bigg and Middleman (1974b) indicate that, except for very large viscosity ratios, a difference in the viscosities of the fluids being mixed retards mixing.

Large amounts of elasticity may distort the flow kinematics significantly, making the applicability of results based on the analysis of mixing of Newtonian fluids doubtful. In principle, the mixing of viscoelastic fluids can be treated in a manner as above, although determination of the flow field is very difficult when the fluids are highly elastic. Several attempts to date have been unsuccessful (cf. Tanner, 1982).

The presence of interfacial tension can alter the mixing characteristics of the flow considerably, particularly in the latter stages of mixing. The breakup of droplets in the microflow elements can be treated by means of the framework outlined by Olbricht et al. (1982) and Khakhar et al. (1984). This is a difficult problem and is the subject of ongoing research.

The analysis of mixing in the single screw extruder serves to illustrate the methodology of this approach, and extensions to other mixers with complicated flow patterns are possible with little conceptual modification, provided the essential elements of the flow kinematics are accessible.

Acknowledgment

This work has been supported by National Science Foundation Grant CPE-8117732.

Appendix

Weighted-Residual Solution for Extruder Flow Equations. The nondimensionalized Navier–Stokes equations for steady, uniform, creeping flow in the extruder channel are (see Figure 2b)

$$\epsilon^2\frac{\partial^2 v_1}{\partial x_1^2} + \frac{\partial^2 v_1}{\partial x_2^2} = \epsilon\frac{\partial P^*}{\partial x_1} \tag{A.1}$$

$$\epsilon^2\frac{\partial^2 v_2}{\partial x_1^2} + \frac{\partial^2 v_2}{\partial x_2^2} = \frac{\partial P^*}{\partial x_2} \tag{A.2}$$

$$\frac{\partial^2 v_3}{\partial x_1^2} + \frac{\partial^2 v_3}{\partial x_2^2} = \left(\frac{H}{L}\right)\tan\theta\,\frac{\partial P^*}{\partial x_3} \tag{A.3}$$

where

$$\epsilon = H/W \tag{A.4a}$$

$$x_1 = x/W \tag{A.4b}$$

$$x_2 = y/H \tag{A.4c}$$

The corresponding boundary conditions are

$$v_2 = 0; \quad (\text{for } x_1 = 0,\ 1;\ x_2\epsilon[0,1]) \tag{A.5a}$$

$$v_1 = 0; \quad (\text{for } x_2 = 0;\ x_1\epsilon[0,1]) \tag{A.5b}$$

$$v_1 = -1; \quad (\text{for } x_2 = 1;\ x_1\epsilon(0,1)) \tag{A.5c}$$

For fully developed flow, $v_3 = f(x_1,x_2)$; then using eq A.3 we can easily show $\partial P/\partial x_3 =$ constant. Equation A.3 can be solved analytically (McKelvey, 1962)

$$v_3 = \frac{4}{\pi}\sum_{n=1,3,\ldots}^{\infty}\frac{\sinh(n\pi\epsilon x_2)}{n\sinh(n\pi\epsilon)}\sinh(n\pi x_1) + \frac{24\phi}{\pi^3}\sum_{n=1,3,\ldots}^{\infty}\frac{\cosh\left[\frac{n\pi}{\epsilon}\left(x_1-\frac{1}{2}\right)\right]}{n^3\cosh\left(\frac{n\pi}{2\epsilon}\right)}\sinh(nx_2) - 3\phi x_2(1-x_2) \tag{A.6}$$

(the sign on the last term on the right-hand side of eq A.6 has been corrected from the cited reference).

The equation of continuity is given by

$$\epsilon\frac{\partial v_1}{\partial x_1} + \frac{\partial v_2}{\partial x_2} = 0 \tag{A.7}$$

In terms of a dimensionless stream function Ψ, and a dimensionless vorticity ω, defined by

$$v_1 = \frac{1}{\epsilon}\frac{\partial\Psi}{\partial x_2}; \quad v_2 = -\frac{\partial\Psi}{\partial x_1} \tag{A.8}$$

$$\omega = -\frac{1}{\epsilon}\frac{\partial v_1}{\partial x_2} + \frac{\partial v_2}{\partial x_1} \tag{A.9}$$

the equation of continuity is identically satisfied, and eq A.1–A.3 reduce to (Lamb, 1932)

$$\nabla^2\Psi = -\omega \tag{A.10}$$

$$\frac{\partial\omega}{\partial x_2} = -\frac{\partial P^*}{\partial x_1} \tag{A.11a}$$

$$\frac{\partial\omega}{\partial x_1} = \frac{1}{\epsilon^2}\frac{\partial P^*}{\partial x_1} \tag{A.11b}$$

where

$$\nabla^2 = \frac{\partial^2}{\partial x_1^2} + \frac{1}{\epsilon^2}\frac{\partial^2}{\partial x_2^2}$$

P^* is eliminated by cross-differentiation, to give

$$\nabla^4\Psi = 0 \tag{A.12}$$

where

$$\nabla^4 = \frac{\partial^4}{\partial x_1^4} + \frac{2}{\epsilon^2}\frac{\partial^4}{\partial x_1^2\partial x_2^2} + \frac{1}{\epsilon^4}\frac{\partial^4}{\partial x_2^4}$$

Equation A.12 has to be solved to obtain the velocity profile. The boundary conditions corresponding to eq A.12 are

$$\Psi = \frac{\partial\Psi}{\partial x_1} = 0; \quad (\text{for } x_1 = 0,1;\ x_2\epsilon[0,1]) \tag{A.13a}$$

$$\Psi = \frac{\partial \Psi}{\partial x_1} = 0; \quad (\text{for } x_2 = 0; x_1 \epsilon [0,1]) \qquad (A.13b)$$

$$\Psi = 0; \frac{\partial \Psi}{\partial x_2} = -1; \quad (\text{for } x_2 = 1; x_1 \epsilon (0,1)) \qquad (A.13c)$$

The lack of continuity of $\partial\Psi/\partial n$ on the boundary prevents both homogenization of the boundary conditions and straightforward application of an "interior" weighted-residual method to the resulting non-homogeneous equation. Instead a "mixed" method is used here (Finlayson, 1972) with the residual minimized both on the boundary and in the interior.

In the Kantorovich–Galerkin method (Kantorovich and Krylov, 1964), Ψ is represented by

$$\Psi = \sum_{k=1}^{N} \beta_k(x_2)\sigma_k(x_1) \qquad (A.14)$$

where the σ_k are known functions and the β_k are determined from residual minimization. The advantage of this method over the standard Galerkin method is that it generally requires fewer terms to obtain the same degree of accuracy.

The σ_k are chosen to satisfy the boundary conditions on Ψ at constant x_1. Taking $N = 1$, one possible representation for Ψ is

$$\Psi = C\beta_1(x_2)x_1^2(1 - x_1)^2 \qquad (A.15)$$

where C is an unknown constant, to be determined. Then from the interior residual condition

$$\int_0^1 (\nabla^4\Psi)\sigma_1(x_1)\, dx_1 = 0 \qquad (A.16)$$

we get the condition on β_1 to be

$$\beta_1^{iv} - 24\epsilon^2\beta_1'' + 504\epsilon^4\beta_1 = 0 \qquad (A.17)$$

or

$$\beta_1 = A_1 \cosh(\delta_1 x_2)\cos(\delta_2 x_2) + A_2 \cosh(\delta_1 x_2)\sin(\delta_2 x_2) + B_1 \sinh(\delta_1 x_2)\sin(\delta_2 x_2) + B_2 \sinh(\delta_1 x_2)\cos(\delta_2 x_2) \qquad (A.18)$$

where

$$\delta_1 = 4.15\epsilon; \quad \delta_2 = 2.286\epsilon \qquad (A.19)$$

From the boundary residual condition

$$\int_0^1 \left\{ \left[\frac{\partial \Psi}{\partial x_2} \right]_{x_2=1} + 1 \right\} x_1^2(1 - x_1)^2\, dx_1 = 0 \qquad (A.20)$$

substituting from eq A.15, A.18 into eq A.20, we get

$$C = 21 \qquad (A.21)$$

The constants A_1, A_2, B_1, and B_2 can be evaluated from the boundary conditions on Ψ, eq A.13, to give

$$A_1 = 0$$

$$A_2 = -\delta_1 \sinh(\delta_1)\sin(\delta_2)/[\delta_2^2 \sinh^2(\delta_1) - \delta_1^2 \sin^2(\delta_2)]$$

$$B_1 = [\delta_1 \cosh(\delta_1)\sin(\delta_2) - \delta_2 \sinh(\delta_1)\cos(\delta_2)]/[\delta_2^2 \sinh^2(\delta_1) - \delta_1^2 \sin^2(\delta_2)]$$

$$B_2 = -A_2\delta_2/\delta_1 \qquad (A.22)$$

Nomenclature

a_v = intermaterial area density
$A = L/R_0$
$\mathbf{C} = \mathbf{F}^T \cdot \mathbf{F}$, right Cauchy–Green strain tensor
$\mathbf{D} = (\nabla \mathbf{v} + \nabla \mathbf{v}^T)/2$, rate of deformation tensor
$E = V_\theta/V_{z_{av}}$
F_1, F_2 = functions of K and r (see Chella and Ottino, 1983)
$\mathbf{F} = \nabla_X \chi$, deformation gradient tensor
H = channel depth
$K = R_i/R_0$, ratio of inner and outer cylinder radius
L = length of helical annular mixer
L = length of interface in two-dimensional cavity flow
L = axial screw length in extruder
$\hat{M}$ = initial orientation vector of differential line element
$\{\hat{M}(\mathbf{X})\}$ = set of initial orientation vectors of differential line elements comprising finite material line
MAC = Marker-and-Cell method
$\hat{n}$ = unit vector normal to material interface
$\hat{N}$ = initial orientation vector of differential material plane
$\{\hat{N}(\mathbf{X})\}$ = set of initial orientation vectors of differential plane elements comprising finite material area
P = pressure
$P^* = PH/V_x\mu$, nondimensionalized pressure
Q = volumetric flow rate
$Q_D = V_z WH/2$, axial drag flow in extruder
$Q_P = -WH^3(\partial P/\partial x_3)/12\mu V_z$, axial pressure flow in extruder
r = radial coordinate in helical annular mixer
R_0, R_i = outer and inner cylinder radii in the helical annular mixer
RTD = residence time distribution
s = striation thickness
SFT = "simplified flow theory" (refers to velocity field of eq 1)
$\bar{t}$ = mean residence time
$t^* = V_U t/H$, nondimensionalized time
$v_1 = v_x/V_x$
$v_2 = v_y/V_y$
$v_3 = v_z/V_z$
V_b = extruder barrel velocity
V_U = velocity of moving plate in rectangular cavity flow
$V_x = V_b \sin\theta$, barrel velocity component in transverse extruder channel direction
$V_z = V_z \cos\theta$, barrel velocity component in axial extruder channel direction
$V_{z_{av}} = Q/\pi R_0^2(1 - K^2)$, average axial velocity in helical annular mixer
$V_\theta = \Omega R_0/(K^{-2} - 1)$, tangential velocity component of inner cylinder in helical annular mixer
W = channel width
WATS = weighted average total strain
$x_1 = x/W$
$x_2 = y/H$
$x_3 = z/Z$
$\mathbf{X}$ = initial coordinate vector of material element
z = dimensionless axial length
$Z = L/\sin\theta$, axial extruder channel length

Subscripts

f = final or exit value
0 = initial value
1, 2, 3, θ, ... = components in coordinate directions 1, 2, 3, θ

Greek Symbols

α = specific rate of stretching of material element
$\epsilon = H/W$ (Appendix)
η = intermaterial area stretch ratio
θ = extruder channel helix angle
μ = viscosity
$\phi = -Q_P/Q_D = H^2(\partial P/\partial z)/6\mu V_z$
χ = motion
Ψ = dimensionless stream function
ω = dimensionless vorticity
Ω = rotational speed of inner cylinder in helical annular mixer

Special Symbols

$\cdot$ = material time derivative
$\overline{\ }$ = spatially or cross-sectionally averaged mean value
$\langle\langle\cdot\rangle\rangle = \int d\dot{Q}/Q$, mixing-cup average
O = order of

Literature Cited

Aref, H. *J. Fluid Mech.* **1984**, *143*, 1.
Aref, H.; Tryggvason, G. *Physica* **1984**, *12D*, 59.
Arimond, J. M.S. Thesis, M.I.T., Cambridge, MA, 1984.
Bigg, D.; Middleman, S. *Ind. Eng. Chem. Fundam.* **1974a**, *13*, 66.

Bigg, D.; Middleman, S. *Ind. Eng. Chem. Fundam.* **1974b**, *13*, 184.
Carley, J. F.; Mallouk, R. S.; McKelvey, J. M. *Ind. Eng. Chem.* **1953**, *45*, 974.
Chella, R. Ph.D. Thesis, University of Massachusetts, Amherst, MA, 1984.
Chella, R.; Ottino, J. M. *ACS Symp. Ser.* **1982**, *196*, 567.
Chella, R.; Ottino, J. M. *Chem. Eng. Sci.* **1984**, *39*, 551.
Chien, W. L. Ph.D. Thesis, University of Massachusetts, 1985.
Erwin, L. *Polym. Eng. Sci.* **1978**, *18*, 572.
Erwin, L.; Mokhtarian, F. *Polym. Eng. Sci.* **1983**, *23*, 49.
Finlayson, B. "The Method of Weighted Residuals and Variational Principles"; Academic Press: New York, 1972.
Gailus, D. W.; Erwin, L. *Soc. Plast. Eng. Pap.* **1981**, *XXVII*, 639.
Han, C. D.; Kim, Y. W. *J. Appl. Polym. Sci.* **1975**, *19*, 2831.
Harlow, F. H.; Amsden, A. A. Los Alamos Scientific Laboratory Monograph LA-4370, Los Alamos, CA, 1970.
Kantorovich, L. V.; Krylov, V. I. "Approximate Methods of Higher Analysis"; Wiley: New York, 1964.
Khakhar, D. V.; Chella, R.; Ottino, J. M. "Proceedings IX International Conference on Rheology", Acapulco, Mexico, Oct 1984.
Lamb, H. "Hydrodynamics", 6th ed.; Cambridge University Press: London, 1932.
Maddock, B. H. *Soc. Plast. Eng. J.* **May 1959**, 383.
McKelvey, J. M. "Polymer Processing"; Wiley: New York, 1962.
Middleman, S. "Fundamentals of Polymer Processing"; McGraw-Hill: New York, 1977.
Mohr, W. D.; Saxton, R. L.; Jepson, C. H. *Ind. Eng. Chem.* **1957**, *49*, 1857.
Mokhtarian, F. M.S. Thesis, M.I.T., Cambridge, MA, 1981.
Olbricht, W. L.; Rallison, J. M.; Leal, L. G. *J. Non-Newtonian Fluid Mech.* **1982**, *10*, 291.
Ottino, J. M. *J. Fluid Mech.* **1982**, *114*, 83.
Ottino, J. M. *AIChE J.* **1983**, *29*, 159.
Ottino, J. M.; Macosko, C. W. *Chem. Eng. Sci.* **1980**, *35*, 1454.
Ottino, J. M.; Macosko, C. W.; Ranz, W. E. *Chem. Eng. Sci.* **1979**, *34*, 877.
Ottino, J. M.; Macosko, C. W.; Ranz, W. E. *AIChE J.* **1981**, *27*, 565.
Ottino, J. M.; Chella, R. *Polym. Eng. Sci.* **1983**, *23*, 357.
Pan, F.; Acrivos, A. *J. Fluid Mech.* **1967**, *28*, 643.
Pinto, G.; Tadmor, Z. *Polym. Eng. Sci.* **1970**, *10*, 279.
Schrenk, W. J.; Cleereman, K. J.; Alfrey, T. *Soc. Plast. Eng. Trans.* **July 1963**, 192.
Shearer, C. J. *Chem. Eng. Sci.* **1973**, *23*, 1091.
Sheridan, L. A. *Chem. Eng. Prog.* **1975**, *71*, 83.
Spencer, R. S.; Wiley, R. M. *J. Colloid Sci.* **1951**, *6*, 133.
Tadmor, Z.; Klein, I. "Engineering Principles of Plasticating Extrusion"; Van Nostrand-Reinhold: New York, 1970.
Tanner, R. I. *J. Non-Newtonian Fluid Mech.* **1982**, *10*, 169.

Received for review December 2, 1982
Revised manuscript received June 1, 1984
Accepted October 10, 1984

Diffusivity of Hydrogen Isotopes in Liquid Lithium and in Solid Yttrium

Robert E. Buxbaum* and Ernest F. Johnson

Department of Chemical Engineering and Plasma Physics Laboratory, Princeton University, Princeton, New Jersey 08544

The separation of tritium from liquid lithium at low concentrations is an important problem for fusion technology. One of the most promising techniques for effecting this separation involves sorbing the tritium on solid yttrium metal. Reliable diffusivity data are essential for a realistic evaluation of this technique. This paper reviews the relevant experimental diffusivity data on protium diffusion in liquid lithium, protium diffusion in solid yttrium, and the isotope effect in metals. On the basis of these data and in the light of standard correlations, the following estimates are proposed for the diffusivity of tritium in liquid lithium and in solid yttrium respectively: $\log D_{T-Li} = -9.038 + 1.737 \log T - 110/T$ (cm^2/s) and $\log D_{T-Y} = -2.391 - 2558/T$. The observed diffusivity values are great enough that the sizes of yttrium surfaces needed for tritium gettering in fusion reactors are of quite practicable dimensions.

Scope

It is generally assumed that the first fusion power reactors will use deuterium and tritium as the principal fuels and that tritium will have to be bred by capturing neutrons from the fusion reaction in a blanket containing lithium in some form. The bred tritium must then be separated from the blanket material and introduced into the fusion reactor fuel mix.

From many standpoints, as demonstrated by Buxbaum and Johnson (1980), the simplest and most attractive breeding medium is liquid lithium, and the most attractive tritium recovery medium is solid yttrium metal. However, in the absence of experimental data on test loops, the practicability of this separation system can be gauged only from paper studies, and such studies will be critically dependent on reliable information on the relevant diffusivity properties. This paper presents the best available information on these properties.

The Diffusivity of Tritium in Liquid Lithium

Cussler (1976) has generalized that the diffusivity of any solute in any liquid solvent is a constant approximating 0.7×10^{-5} cm^2/s. While this assertion tends to be accurate within an order of magnitude, a more reliable estimate, polymeric liquids excepted, may be made on the basis of the Nernst–Einstein (Langevin, 1908) equation. A convenient simplification of this equation is the Stokes–Einstein equation (Einstein, 1956), viz.

$$\mathbf{D} = kT/6\pi\bar{r}\mu \qquad (1)$$

where k is Boltzmann's constant, 1.3805×10^{-13} N-cm/K, T is absolute temperature, k, μ is the solvent viscosity, n-s/cm^2, and $\bar{r}$ is the effective radius of the diffusing species, cm. For relatively spherical molecules

$$\bar{r} \simeq (3V/4\pi N_{Av})^{1/3} \qquad (2)$$

where V is the molecular volume at the normal boiling point, cm^3/g mol, and N_{Av} is Avogadro's number, 6.02×10^{23} molecules/g-mol. For nonspherical molecules, the effective radii may be determined from pseudo-steady hydrodynamic mobilities (Brenner, 1974).

The effective radius of the lithium hydride molecule is found to be 1.7 Å, when calculated from eq 2. This radius, when inserted into eq 1, does not correlate well with experiment, presumably because the diffusing species is not the lithium hydride molecule. Rather, hydrogen diffuses in liquid lithium as Li_2H molecules, Li_3H molecules, or possibly as larger conglomerates.

*Department of Chemical Engineering, Michigan State University, East Lansing, MI 48824.

0196-4313/85/1024-0180$01.50/0